Chapter 2

Molecular Plasmonics: From Molecular-Scale Measurements and Control to Applications

Bharath Bangalore Rajeeva and Yuebing Zheng*

**Materials Science and Engineering Program,
Department of Mechanical Engineering, The University of Texas at Austin,
Austin, Texas 78712, United States
*E-mail: zheng@austin.utexas.edu.**

Nanophotonics is a prominent field within nanotechnology aimed at researching the light-matter interactions occurring at the nanoscale. In case of metal nanostructures, collective oscillation of electrons leads to nanoscale confinement of optical fields with high thermal energy and elevated near-field optical forces. The interactions of these effects with molecules known as molecular plasmonics have generated novel devices with implications in energy, biology, and healthcare. In this chapter, we will review our research on molecular plasmonics in three correlated sections: molecular-scale measurements and control, directed and self-assembled nanofabrication, and real-life applications. The first section presents the measurements and control of molecular-scale events using active molecules as a framework. We further summarize two unconventional nanofabrication techniques based on directed and self-assembly, i.e., moiré nanosphere lithography and multi-photon plasmonic lithography. The success in these two arenas positions molecular plasmonics to be propelled for real-life applications. We finally present the potential of plasmonics in achieving its promise of creating futuristic technologies.

Cheng et al.; Nanotechnology: Delivering on the Promise Volume 2
ACS Symposium Series; American Chemical Society: Washington, DC, 2016.

1. Introduction

Tasks which were once inconceivable are now commonplace due to rapid technological advancements. Specifically, the curiosity to understand and develop novel phenomena and devices has led to multidisciplinary convergence of scientists to explore and develop nanotechnology. Nanotechnology focuses on the study and manipulation of unique fundamental property differences that originate when the size of material is scaled down to a collection of several atoms. Advancements in nanotechnology have been steered by the ability to fabricate, measure and optimize nanoscale structures using sophisticated tools. Among its various research areas, nanophotonics has been an active and prominent field due to the interesting optical properties that arise at sub-wavelength scales. Traditionally, it has been challenging to study the optical interactions at the nanoscale due to the diffraction limit, which restricts the focusing of light to dimensions roughly above one half of the wavelength. This barrier has been overcome in the past decades, leading to intense research in the area of nanophotonics.

Nanophotonics aims to design and manipulate the behavior of optical field at the scale of a fraction of the wavelength. Research on nanophotonics has resulted in immense applications in various realms such as optical fiber technology, solar energy conversion, molecular diagnosis and therapy, and biosensors. According to Forbes, market for nanophotonic components and devices has been projected to reach $100 billion (*1*). In the past two decades, nanophotonics has been primarily approached by the following three strategies: (i) confinement of light waves in various structures, (ii) confinement of atoms to create materials in the sub-100 nm regime, and (iii) characterization and control of photophysical and photochemical processes at the nanoscale. Based on the above strategies, two prominent areas in nanophotonics being investigated are photonic crystals and plasmonics.

1.1. Photonic Crystals and Plasmonics

Photonic crystals (PCs) are periodic dielectric nanostructures with lattice parameters comparable to the wavelength of light. The periodic modulation of the dielectric medium creates photonic band gaps or stop gaps, which limit the propagation of certain wavelengths of light. The refractive-index contrast between the materials, structural symmetry and lattice parameters of the particles can be altered to tune the bandwidth and frequency of PCs. The transmission and reflection properties of PCs can be rationally designed by using modeling methods involving either plane-wave expansion (*2*), or transfer matrices (*3*) of the Maxwell equation. PCs have found applications in a variety of industries such as telecommunications (PC fibers, and integrated optical components), medicine (micro-lasers, and biosensors), and displays (image sensors). A recent market report estimated PC component market as $6 billion in 2014, with a projection to reach $17.4 billion in 2020 (*4*).

Plasmonics involves the study of the interaction between electromagnetic radiations and free electrons of a metal. In general, materials which possess a negative real and a small imaginary dielectric constant can support a surface

plasmon resonance (SPR). SPR is the coherent oscillation of the free electrons in response to an incident electromagnetic radiation, and has achieved prominence due to its ability to circumvent the diffraction limit. SPR has important applications in surface-enhanced spectroscopies (*5*) and biological sensing (*6*). With molecular spectroscopy market projected to reach $5.9 billion by 2018, plasmonics is expected to make significant contributions. For instance, commercial instruments such as BIAcore® employ SPR spectroscopy to monitor thermodynamics and kinetics of biological binding processes (*7*).

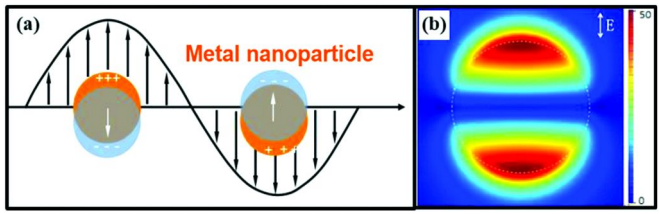

Figure 1. (a) Schematic illustration of localized surface plasmon at metal nanoparticles. (b) Optical simulation shows the hot spots of an Ag nano-disk on a substrate upon incidence of electromagnetic radiation at plasmon resonance. Reproduced with permission (8). Copyright 2015 Springer Science+Business Media New York.

SPR can exist either as propagating or localized surface plasmon. Surface plasmon polaritons (SPPs) are electromagnetic excitations which occur at a metal/dielectric interface. They propagate parallel to the surface, but decay exponentially in both media along the perpendicular direction. This property can be exploited to localize and guide light in subwavelength metal structures to fabricate nanoscale optoelectronic circuits and components (*9*). For sensing applications, the interaction between the SPP and the molecular surface layer results in plasmon resonance shift, which can be characterized via reflectivity measurements as a function of either wavelength or incident angle (*10*). In the case of localized surface plasmon resonances (LSPRs), light interacts with nanoscale particles which are smaller than the incident wavelength (Figure 1), leading to the light-coupled coherent oscillation of electrons confined within the nanoparicle (NP). The LSPR is extremely sensitive to local dielectric environment, which can be sensed via a wavelength shift. The excitation of LSPR creates localized enhancement of electromagnetic fields in the vicinity of the NP. Figure 1(b) shows the field enhancement around a 10nm Au NPs.

1.2. Molecular Plasmonics

Molecular plasmonics fuses light and molecules at the nanoscale. In this emerging field, one exploits the plasmon-enhanced nanoscale light for molecular analysis or seeks the synergy of the response of molecules and the nanoscale light manipulation by surface plasmons for active nanophotonic devices. For example, the light confined at the nanoscale can interact with cells

and biomolecules of variable sizes. An efficient control and understanding of the interactions (optical, thermal and mechanical) between the molecules and SP can lead to superior sensing, trapping and manipulation at molecular and cellular levels (*11–15*). For instance, the high scattering and absorption cross sections help improve the sensitivity of molecular spectroscopy (*16*). The promising developments in nanolaser, non-linear quantum optics, terahertz nanoelectronics and ultra-high fluorescence enhancements have also been enabled by harnessing the plasmon-molecule interactions (*17–19*). The success of molecular plasmonics has been and will continue to be contingent upon simultaneous development of plasmonic and molecular nanotechnology.

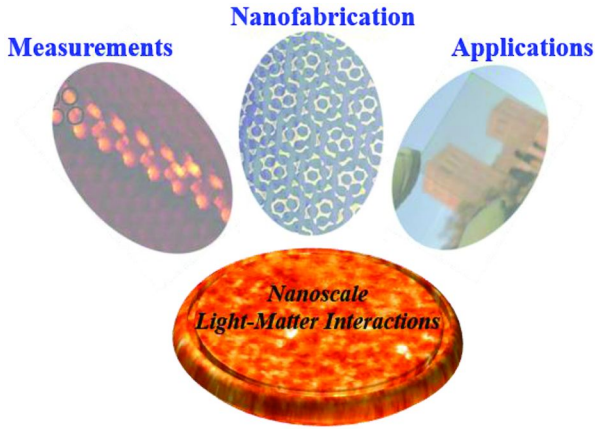

Figure 2. An overview of book chapter focused on our fundamental study and applications of molecular plasmonics and nanoscale light-matter interactions: (i) molecular-scale measurements and control, (ii) directed and self-assembled nanofabrication, and (iii) applications in energy, biology and healthcare.

In this chapter, we review our research on molecular plasmonics and the applications of plasmonics in the domains of energy, biology, and healthcare. As shown in Figure 2, the chapter is divided into three synergistic sections. The first section concentrates on the methods and tools available for the measurements and control of molecules. These techniques are essential for the understanding of molecular-scale processes and for the scaling-up of molecular units for device applications. We exploit the sophisticated measurement tools to study active molecules such as rotaxane and azobenzene, which can change their properties in response to external stimuli. The second section discusses a couple of unconventional nanofabrication techniques based on directed and self-assembly, including moiré nanosphere lithography (M-NSL) and multi-photon plasmonic lithography (MPPL), which provide versatility and cost-effectiveness in nanofabrication. The final section provides a snapshot of our recent work on the applications of plasmonics in the energy, biology, and healthcare.

2. Molecular-Scale Measurements and Control

Due to the extremely small size of molecules, it is imperative to have tools that are capable of measuring events at the scale of few nanometers. The ability to resolve and separate the plasmonic and molecular changes is beneficial. To this end, imaging techniques such as scanning electron microscopy (SEM), atomic force microscopy, scanning tunneling microscopy (STM), and near-field optical scanning microscopy have been developed. Further, optical characterization techniques such as single-particle dark-field scattering spectroscopy, surface-enhanced Raman spectroscopy (SERS) and tip-enhanced Raman spectroscopy have emerged. In this section, we summarize our approaches towards the nanoscale characterization of active molecules using STM and SERS. Our progress in developing controlled molecular environments based on directed and self-assembly techniques are also summarized.

2.1. Self-Assembly

Self-assembly is an attractive strategy to obtain surface functionalization in a controlled, organized manner via the tuning of the molecule-molecule and molecule-substrate interactions. It is defined as the spontaneous assembly of molecules into structured, stable, non-covalently joined aggregates under equilibrium (*20*). Typically self-assembly has been employed for creating monolayers of molecules (*21*) or polymer micro/nanoparticles (*22*). Due to its ease of preparation, high versatility, high throughput, and low cost, self-assembly of molecules has been used for numerous applications beyond the surface functionalization (*23*), including molecular electronics (*24*) and biomolecule immobilization (*25*). Self-assembled monolayers (SAMs) of thiols on Au are one of the well-researched platforms due to their high stability in the ambient atmosphere and their ability for precise modification (*21*, *26–28*). At relatively low concentrations of ~1mM, ethanolic solution of thiols swiftly organize on Au surfaces via covalent bonds formed between the thiol head group and Au. The tail groups are exposed in ordered lattices and a few types of disorders or defects, including step edges, vacancy islands, and monolayer defects (tilt domain boundaries and improper ordering of molecules) exist. Figure 3 depicts the scanning tunneling microscopy image of decanethiol SAMs on Au{111} along with the marked defect regions (*29*).These defects in SAMs are exploited to position desired active molecules with precise placement and orientation control (*30*, *31*).

Molecules are inserted onto the SAMs in the solution and vapor phases, as well as through microcontact insertion printing. In most scenarios, SAMs with thickness of few nanometers are ideal for molecular plasmonics. Further, these molecules have a tendency to preferentially attach at the defect sites in the SAMs since these are the most reactive and sterically accessible sites on the Au surface (*32–34*). SAMs can also be applied to functional molecules. For example, to extend the applicability of rotaxanes, we formed the SAMs on Au surfaces through the modification of rotaxanes with disulfide-based anchoring groups (*35*). The SAMs enable the applicability of molecular machines by facilitating their

coordinated functioning at the nanoscale. In another example, Huang, Weiss, Stoddart, and co-workers utilized SAMs of rotaxane molecules on Au surfaces to drive a mechanical cantilever (*36*).

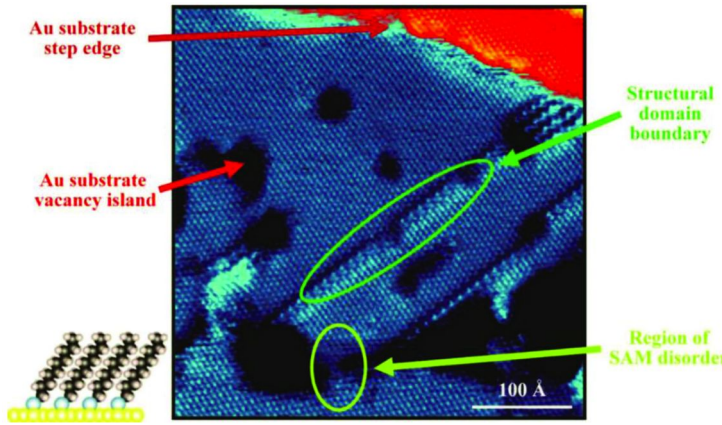

Figure 3. Scanning tunneling micrograph of decanethiol SAM on Au{111} surface depicting the various types of defects such as step edges, vacancy islands, improperly ordered molecules, and tilt domain boundaries. Reproduced with permission (29). Copyright 2008 American Chemical Society.

2.2. Scanning Tunneling Microscopy

The ability of characterizing the properties of molecules on surfaces is of great interest. For instance, it is crucial to understand whether the molecules retain their functionality when positioned on surfaces (*37*). While techniques such as cyclic voltammetry (*38*) and X-ray photoemissions spectroscopy (*39*) are useful for ensemble measurements, to achieve single-molecule resolution to gain significant insights is plausible with STM. STM can be used for imaging surfaces at an atomic resolution (*40*). STM measurements can be used to estimate the insertion efficiency, arrangement and orientation of molecules on surfaces, providing information about the quality of the SAMs. STM can also monitor conformational changes in active molecules (e.g., molecular switches and motors) upon exposure to external stimuli. In order to obtain statistically significant data, a large number of measurements are needed from the sites of interest (*41*). Because the activity of individual active molecules can be altered by the environment and the neighboring active molecules (*29*, *42*, *43*), it is imperative to isolate and characterize individual molecules in controlled environments.

Weiss and co-workers have achieved isolation of single molecular motors and switches in ordered alkanethiol SAM matrices (*30*, *31*, *44*, *45*). STM images are recorded as the convolution of topography and electronic properties of the molecules. The images provide the apparent height profile of active molecules relative to the SAM matrix (*46*), and can be used to study molecular switching at an ultra-high resolution. As an example, Figure 4 shows the schematic of azobenzene

undergoing reversible photoisomerization within the alkanethiol domain. The use of 1-decanethiol as the matrix ensures that the azobenzene molecules protruding out of the matrix have ample degrees of freedom for structural changes to occur (*30*). The inserted azobenzene-functionalized molecules within alkanethiol monolayer also limits the stochastic switching events which are otherwise observed due to the movement of molecules bound at the defect sites (*32*, *45*, *47*). The co-deposition is performed by immersing annealed Au substrates in a solution of azobenzene and alkanethiol at a temperature of 80 °C. This leads to the insertion of azobenzene molecules within the ordered alkanethiol domains.

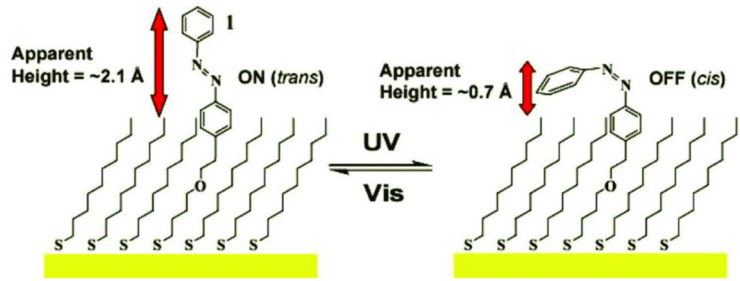

Figure 4. Isolated single azobenzene molecules embedded in a matrix of 1-decanethiol over Au {111} surface. The photoisomerization results in a change from 2.1±0.3 Å to 0.7±0.2 Å with respect to the SAM matrix upon switching from trans to cis form. Reproduced with permission (30). Copyright 2011, American Chemical Society.

The isolated active molecule within the matrix is characterized by a STM which is equipped with a light source to irradiate the tunneling junction while the scanning tip is still present. This ensures the on-demand illumination of azobenzene molecules for specific periods of time along with continued imaging. Figure 5 summarizes the conformational changes of azobenzene under different irradiation conditions. Initially, the individual trans-azobenzene molecules possess an apparent height of ~2Å with respect to the SAM matrix. Upon UV (365nm) irradiation, the molecules gradually change the apparent height with an increase in the exposure time. The reduction in apparent height to ~0.7 Å upon photoisomerization is a result of (i) lower conductance of cis-azobenzene with respect to trans since it is non-planar, and (ii) change in the height of the molecule after the isomerizstion. The cis form can return back to the thermodynamically stable trans orientation through visible light illumination. This phenomena is observed in Figure 5 (F) where some of the molecules revert back to the trans conformation after 30mins of visible light exposure. STM imaging has been performed on other alternative substrates such as GaAs (*48*).

Although the measurements on single molecules provide valuable insights into the physics and chemistry at the nanoscale, real-life devices mandate a large number of molecules in one-dimensional (1D), two-dimensional (2D) and even three-dimensional (3D) assemblies, which involve intermolecular interactions and charge transport (*29*, *49*, *50*). The 1D assemblies are obtained

via the assembly of compact azobenzene molecules assembled around the domain boundaries of 1-decanethiol monolayers (*51*). In this scenario, we observe a reduced switching speed although all molecules undergo switching coherently. This suggests the presence of electronic coupling along the chain. By exploiting the cooperative functions, it is plausible to create novel 2D assemblies with superior photoswitching capabilities (*52–54*).

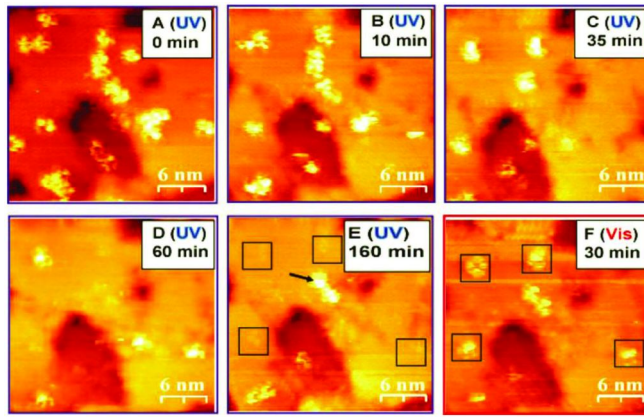

Figure 5. STM images of azobenzene molecules in SAM matrix upon irradiation with UV (~365nm) light for (A) 0 min, (B) 10 min, (C) 35 min, (D) 60 min, and (E) 160 min, as well as subsequently under visible light (~450nm) exposure for (F) 30 min. The images show the switching of azobenzene between high-conductive trans and low-conductive cis forms. STM imaging was performed with V_{sample} = 1V and I_t = 2pA. Reproduced with permission (30). Copyright 2011, American Chemical Society.

2.3. Surface-Enhanced Raman Spectroscopy

Since the first report on single-molecule SERS in 1977 (*55*), intense research in various disciplines, including physics, chemistry and life sciences, has led to the rapid development of SERS over the past two decades. SERS is a nanoscale phenomenon where the enhancement in Raman signal is observed due to the coupling between vibrational modes of the molecule and the LSPR of the metal nanostructure upon optical excitation (*56*). It has immense applications in a plethora of avenues such as biosensing (*57*) of various diseases such as cancer (*58*, *59*) and Alzheimer's disease (*60*, *61*), spectroelectrochemistry (*62*), chemical warfare agent detection (*63*), and single-molecule SERS (*64*). SERS provides a comprehensive information on the vibrational modes of the molecule along with high sensitivity towards conformational changes (*65*). By exploiting the surface selection rules that vibrational modes perpendicular to the substrate are enhanced while parallel modes remain constant, it is possible to obtain information regarding the orientation of the molecule on a specific substrate (*66*, *67*).

Specific to active molecules, SERS provides a unique opportunity to probe ensemble averages of the molecular events. As an example, we have employed SERS to study photoisomerization of alkanethiolate-tethered azobenzene inserted in dodecanethiolate SAM matrix. The host-guest structures and tethers help reduce the surface quenching and steric hindrance for photoswitching of molecules on metal surfaces (*68*). The nanohole arrays on Au{111}/mica were carefully designed to provide the necessary field enhancement to obtain large SERS intensity (Figure 6) (*45*).

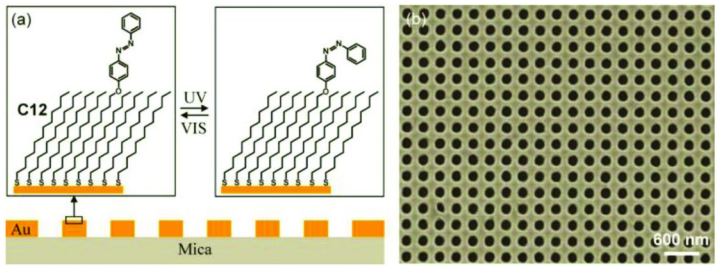

Figure 6. (a) Schematic illustration of the cross-sectional view of azobenzene molecule inserted in the dodecanethiolate SAM matrix on Au {111} with nanohole arrays. (b) SEM image of the nanohole array on Au {111}. Reproduced with permission (45). Copyright 2011, American Chemical Society.

The SERS spectra obtained at specific time intervals of alternating UV and blue light irradiation on the molecules are shown in Figure 7. The vibrational modes that contribute to different Raman peaks denoted as C1-C5 are illustrated in the diagrams in the lower panel. The switching characteristics are analyzed by processing the ratio of the peak areas of each spectrum. From the data for various Ci/Cj (i,j in the range of 1-5), we observe a monotonic and reversible trend in the peak-area ratio (C3:C4) upon alternative UV and blue light exposure (Figure 7d). The peak ratio is decreased upon UV irradiation (*trans* to *cis* transformation) and blue light switches it back to *trans*, which is manifested as an increase in C3/C4 ratio. Unlike STM, SERS tool enables ensemble measurements of isolated molecules and assemblies in controlled nano-environments. SERS can be exploited to understand many other types of active molecules and their functional devices (*69*). In a separate work, we have utilized SERS to probe the reaction pathways for self-assembled anthracene molecules on Au substrate, and study the influence of nanoscale morphology on the regioselective reactions (*70*). It is possible to further gain dynamic information by integrating SERS with ultra-fast optics (*71*). With recent developments in the creation and manipulation of hot spots, SERS can be efficiently employed for studying molecule-plasmon interactions at high spatial and temporal resolution (*72*).

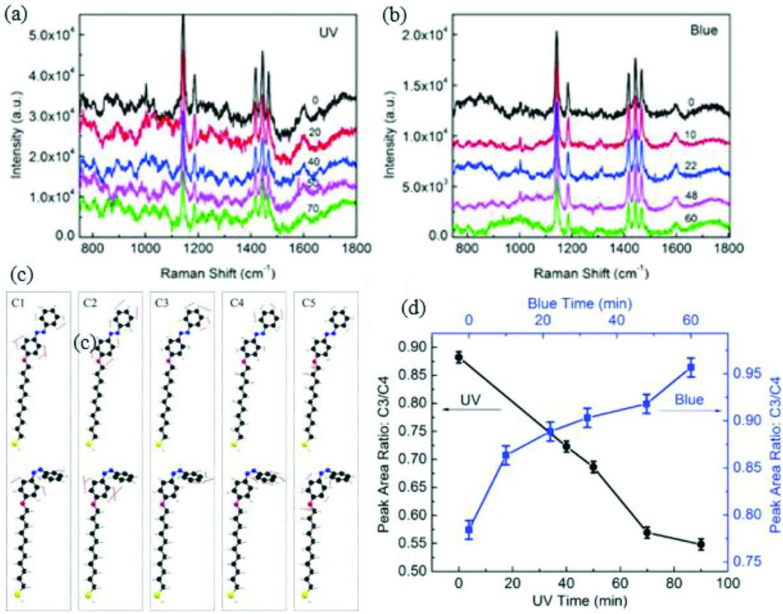

Figure 7. A series of time-dependent SERS spectra of azobenzene obtained after alternate exposure of (a) UV (~350nm) and (b) blue (~450nm) light over the sample. The spectra are shifted along the y-axis for clarity. (c) Schematic showing the varous modes (C1-C5) for trans and cis configuration. (d) Experimental C3/C4 Raman peak ratio as a function of UV and blue light exposure times. Reproduced with permission (45). Copyright 2011, American Chemical Society.

3. Directed and Self-Assembled Nanofabrication

Progress in nanofabrication techniques has been an integral component for propelling the research in nanophotonics. It involves making functional structures with well-defined features having the least dimension to be <100 nm. Majority of the patterning has been accomplished via photolithography, and has been primarily aimed at the semiconductor industry. Over the years, varioius nanofabrication techniques have been developed in parallel to combat the high cost and diffraction limit of light in photolithography and to fabricate complex 2D and 3D structures for novel optical properties. Scanning beam techniques such as electron-beam lithography and focused ion-beam lithography can create arbitrary precise features. However, they feature low throughput since patterns are carved out line-by-line with high-energy (>10 kV) electron and ion beams. These limitations have motivated researchers to further explore the unconventional nanofabrication techniques based on directed and self-assembly. In this section, we highlight our research on M-NSL and MPPL.

3.1. Moiré Nanosphere Lithography

Over the past two decades, nanosphere lithography (NSL) has emerged as a low-cost, large-scale nanofabrication technique for creating periodic nanostructures. NSL, which is also known as colloidal lithography (*73*) or natural lithography, is a method of organizing nanospheres into tightly packed patterns to aid the creation of metasurfaces and nanostructures (*74*). The patterns obtained by metal deposition using the monolayer of nanospheres as the mask feature hexagonal arrays of metal nanotriangles (*75*). The use of bilayer sphere as masks leads to quasi-spherical NPs (*76*). With a variable combination of materials deposition and etching steps, it is possible to create myriads of structures such as nanodisks (*77*, *78*), nanorings (*79*), nanopillars (*80*, *81*), and nanoholes (*82*, *83*). A few variants of NSL such as angle-resolved NSL and shadow NSL have emerged (*84*, *85*). They involves the dynamic and non-dynamic deposition of materials at non-zero incident angle with respect to the substrate normal. This can result in exotic shapes such as nanooverlaps, nanogaps, nanochains, and nanocups. The major motivation for the creation of these periodic metal nanostructures is to exploit their plasmonic properties. These nanostructures have proved as strong candidates for applications in surface-enhanced spectroscopy, photocatalysis (*86*), and biochemical sensing (*87*). In the context of active molecular plasmonics, we have employed nanodisk arrays to study the tunable plasmon-exciton resonant coupling, which has potential applications in active nanophotonic devices (*88*, *89*).

Recently, we have developed M-NSL to further extend the capability of NSL in fabrication of novel nanostructures (*90*). Conventional NSL involves convective self-assembly of nanospheres, in which colloidal spheres assemble into crystalline patterns as a result of capillary and hydrodynamic forces. M-NSL is a modified version of NSL, which can be used to create complex nanostructures with moiré patterns by depositing layers of close-packed spheres one at a time and applying an in-plane rotation between the layers. Figure 8 illustrates the spontaneous self-assembly of bilayers in NSL and the layer-by-layer deposition of bilayers in M-NSL.

Depending on the relative in-plane rotation between the top and bottom layers, the resultant moiré patterns vary. With a small angle of rotation (<10°), the moiré patterns have a large unit cell with simple structures. As the angle increases to 10°- 30°, the moiré patterns have a smaller unit cell with increased complexity. Once the angle of rotation is larger than 30°, the patterns start to repeat due to the symmetry of the two layers. Figure 9 shows the low- and high-magnification SEM images of the plasma-etched M-NSL bilayer with moiré pattern. Like NSL, the M-NSL bilayers can be used as lithographic masks to create various metal nanostructures on general substrates. The resultant metasurfaces exhibit tunable multiband optical responses ranging from visible (~600 nm) to mid IR (~4200 nm), enabling their applications in ultrabroadband absorbers and multiband SERS substrates (*91*).

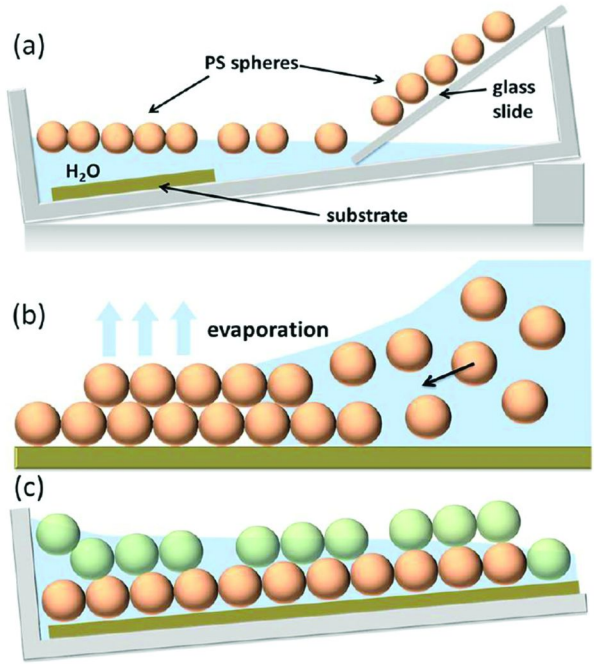

Figure 8. (a) Schematic of the formation of monolayer of polystyrene spheres at water-air interface and its transfer to glass slide. (b) Schematic of spontaneous self-assembly of bilayer of spheres in NSL. (c) Schematic of layer-by-layer stacking of spheres with the in-plane rotation in M-NSL. The different colors indicate the angle rotation between the top and bottom layers. Reproduced with permission (90). Copyright 2015, American Chemical Society.

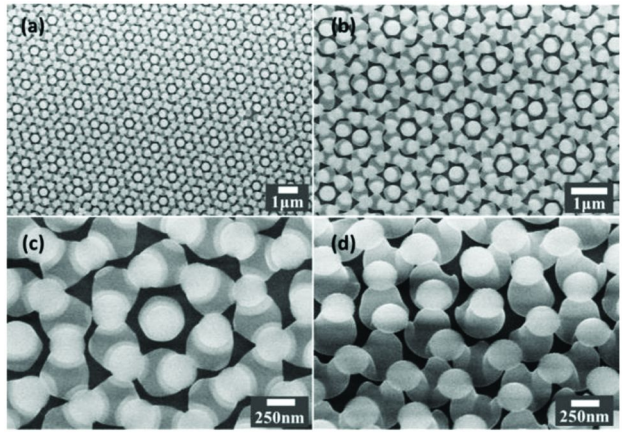

Figure 9. (a-c) SEM images of the etched bilayer in M-NSL with different magnifications. (d) 30° tilted view of the bilayer. Reproduced with permission (90). Copyright 2015, American Chemical Society.

3.2. Multiphoton Plasmonic Lithography

In recent years, multiphoton fabrication (MPL) has emerged as a powerful technique for direct laser writing of complex 3D structures with resolutions beyond the diffraction limit (*92*). This is typically achieved by scanning a tightly focused beam of a femtosecond laser inside polymer materials. The unique aspect of MPL is that the photo-crosslinking occurs at the vicinity of the focal point, where the laser intensity is high enough for photoreactants to absorb two or more photons simultaneously, a process known as non-linear absorption. This high localization of reaction and freeform fabrication capability has been utilized to create novel photonic devices (*93*). The dependence of MPL on the intensity threshold has motivated researchers to couple MPL process with plasmonics, resulting in the development of MPPL. MPPL relies on the fact that LSPR can be used to trigger and control photophysical and photochemical reactions, which occur via the coupling between the LSPR energy and the chemical system (*94*).

The metal NPs have intense field enhancements at the plasmonic hot spots, which lead to an enhanced energy density exceeding the non-linear absorption threshold of polymers within these regions. The nanoscale confinement of the hot spots has been utilized to fabricate highly resolved nanostructures using photoresists such as SU-8 and TSMR-V90 (*95*). It has also been used to visualize the plasmon modes in nanostructures (*96*) and to enhance SERS performance via selective adhesion of molecules within the hot spots (*97*). MPPL has also been used in conjunction with atomic force microscopy to visualize the non-resonant electromagnetic effects in Au nanorods (*98*).

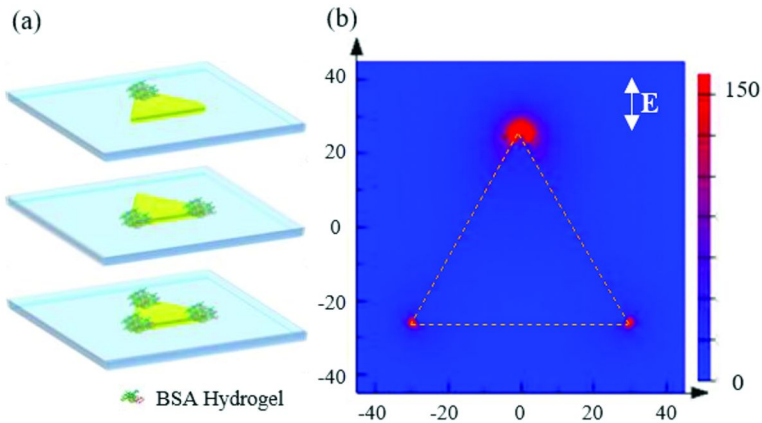

Figure 10. (a) Schematic showing the immobilization of BSA hydrogel on the one, two and three tips of a single AuNT (b) The FDTD simulated field-intensity distribution over a single AuNT upon incidence on linearly polarized light. The intensity enhancement ($|E|/|E_0|$) is shown in the color scale.

We have recently extended the capability of MPPL to regioselectively localize protein molecules at the hot spots of a single Au nanotriangle (AuNT) (*99*). We direct bovine serum albumin (BSA) hydrogels at the tips of a single AuNT

along with control over their position and quantity. In MPPL, the intensity and polarization of incident light was tuned to achieve BSA hydrogel localization at one, two and three tips of a single AuNT (Figures 10a). Specifically, Rose Bengal, the photosensitizer used in the fabrication medium undergoes facile intersystem crossing within the plasmonic "hot spots", which promote the intermolecular BSA crosslinking through singlet-oxygen and/or direct hydrogen-transfer mechanism (*100*). In Figure 10 (b), simulated data using finite-difference time domain (FDTD) method depict the hot spot present at the tips of the AuNT when irradiated with linearly polarized light. The regioselective process was further characterized using single-particle dark-field scattering spectroscopy. With the extension of MPPL to biological domains, we envisage the use of the hybrid metal-biomolecule nanostructures for the better understanding of various biological processes at the nanoscale such as cell-matrix interactions. With the better understanding and finer control, MPPL will significantly impact nanophotonics by enabling various novel nanostructures such as tunable nanoantennas, nonlinear nanostructures, and protein-based micro-lens (*101*).

4. Applications in Energy, Biology, and Healthcare

Novel and exciting applications arise from the intriguing photonic phenomena at the nanoscale. The engineering of size, shape and composition of metal NPs can lead to different kinds of optical responses. As a result of the extensive research over the past two decades, plasmonics is on the verge of delivering its promise of transforming various basic research and industries such as healthcare, energy and telecommunication. In the first sub-section, we discuss our research aimed at the exploitation of plasmonics in solar-energy harvesting technologies such as photoelectrochemical (PEC) cells and transparent solar cells. The second sub-section focuses on the applications in biology and healthcare sectors, with an emphasis on the development of point-of-care devices. One of the most promising biological applications of plasmonics is in biosensors, whose industry is projected to grow from $13 billion in 2014 to $22.5 billion in 2020 (*102*).

4.1. Solar-Energy Harvesting

With an ever-increasing energy demand, the need for harnessing alternative sources of energy has become inevitable. Over the past few decades, technologies utilizing the incident solar radiation have resulted in significant environmental benefits and sustainable development. The solar energy is utilized primarily by its conversion to either electrical energy (photovoltaic), chemical energy (photocatalysis) or heat energy (solar heaters). For creation of viable technologies, it is critical for the devices to achieve a high conversion efficiency. Among the various approaches for efficiency enhancement, the ability of metal NPs to concentrate electromagnetic fields, along with the option of engineering the scattering and absorption of radiation, makes them an efficient medium for enhancing the device performance.

PEC water splitting is a promising technology, which mimics natural photosynthesis to generate chemical fuels such as hydrogen and oxygen using solar energy. Traditional PEC cell employs a semiconductor photoelectrode and a metal counter electrode. Although the concept was introduced in 1972 (*103*), real-life applications of robust and efficient PEC cells have been limited. The criteria for achieving a high performance include: (i) a high absorption of solar radiation obtained via appropriate band energies and structures, (ii) low electron-hole pair recombination, (iii) a high charge-carrier conductivity, and (iv) a fast surface reaction kinetics. Since most of the semiconductors fail to meet all the requirements, inclusion of plasmonic NPs can offset the limitations (*104*). Semiconductors such as TiO_2 and ZnO with wide band gaps (UV absorption) can be sensitized to utilize visible light via absorption and subsequent electron transfer from Au NPs to the semiconductors. For instance, Li and co-workers have demonstrated photoactivity over an entire UV-visible spectrum on TiO_2 by incorporating Au NPs (*105*). A similar effect with increased absorption has been observed on ZnO (*106*). Recently, absorption of 27% of solar radiation in 300-1100 nm has been achieved using Ag-Si nanocones (*107*). Further, metal NP can act as an antenna to localize optical energy at the semiconductor-NP interface. This can reduce the travel distance of minority charge carriers, thereby limiting recombination (*108*). Integration of large NPs with efficient scattering can increase the path length of the incident light. The cumulative effects improve device efficiency and reduce active semiconductor volume.

The mechanisms for plasmonic enhancement include (i) plasmon resonance energy transfer (PRET) from metal NPs to the adjacent semiconductors via dipole-dipole interactions. This was exploited by Cronin and co-workers to achieve 66 times enhancement in photocurrent with Au-TiO_2 anode under 633 nm irradiation (*109*); (ii) hot-electron injection, where electrons are generated in the Au NPs and injected into the conduction band of semiconductors upon non-irradiative decay of surface plasmons. This mechanism is possible only when the metal NP and semiconductor have direct contact, resulting in a Schottky barrier with the work function of the metal NPs higher than that of an n-type semiconductor or lower than that of a p-type semiconductor. This mechanism has proved to enhance performance in titanium oxide (*110*), zinc oxide (*111*), cerium oxide (*112*), and tungsten oxide (*113*); (iii) plasmonic heating, which in most situations has a minor role; and (iv) local electromagnetic field concentration for the enhanced light absorption by semiconductors (*114*, *115*).

For a further reduction in cost and improvement in performance, the earth-abundant, stable and visible-light active photoanodes of metal oxides such as haematite (Fe_2O_3) and bismuth vanadate ($BiVO_4$) are being explored. Among these photoanode candidates, $BiVO_4$ is a promising material due to a direct band gap of 2.4 eV and suitable band position for oxygen evolution, which lead to a low onset potential and utilization of blue portion of the visible spectrum (*116*). Compared to bulk $BiVO_4$, which suffers from high charge recombination, nanostructured $BiVO_4$ along with co-catalyst has been reported to achieve high photocurrent density of 2.73 $mAcm^{-2}$ at a potential as low as 0.6 V versus reversible hydrogen electrode (RHE) (*117*). In addition, we have demonstrated the role of hydrogen treatment in improving $BiVO_4$ performance, which is

attributed to the enhanced carrier density and conductivity (*118*). Further, Zhang and co-workers demonstrated the plasmonic enhancements in $BiVO_4$ photonic crystals (*119*). Recently, we have demonstrated Au-NP-decorated nanoporous $BiVO_4$ photoanodes in which we synergize multiple enhancement mechanisms, including enhanced charge and carrier collection, plasmon-induced electron and energy transfer, and plasmon-enhanced electromagnetic field (*120*). Figure 11 shows scanning electron micrograph of the Au-BiVO4 photoanode. The high-resolution transmission electron micrograph (inset of Figure 11) reveals the Au nanoparticles.

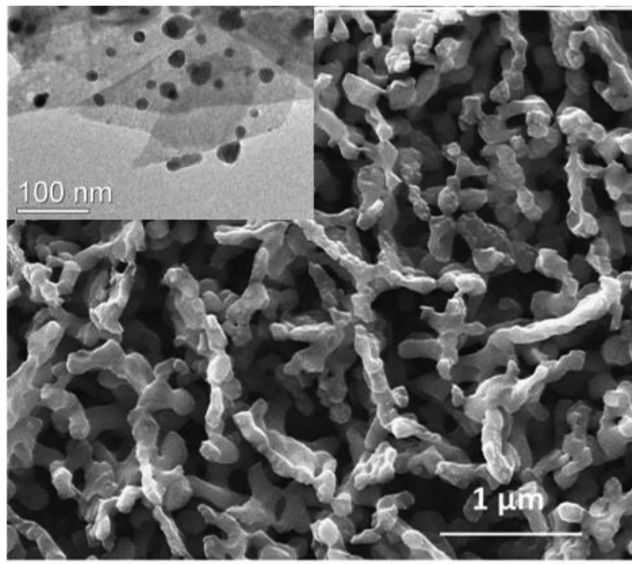

Figure 11. Scanning electron micrograph of Au-BiVO4 photoanode. Inset is the high-resolution transmission electron micrograph revealing the Au nanoparticles.

Photovoltaics, the most prominent application of solar-energy harvesting also benefits from the unique properties of metal NPs. Similar to their advantages in PEC cells, plasmonic nanostructures can enhance light absorption and scattering as well as reduce light reflection (*121*). In addition, they can serve as back contact of solar cells and aid in the creation of transparent solar cells (*122*). We have demonstrated transparent polymer solar cells (with an efficiency of 4%) with Ag nanowire networks as electrodes (*123*). A further exploitation of plasmonic effects in the electrodes could improve the efficiency. By creating or improving

next-generation energy materials, plasmonics is expected to play a pivotal role in enhancing our energy-harvesting capabilities.

4.2. Biology and Healthcare

Intense research on plasmonic materials has greatly benefited biomedical -- and healthcare sectors. Numerous applications such as multifunctional theranostics and ultra-sensitive portable multi-assay biosensors have been realized (*124*). The enhanced photo-thermal effects have gained prominence for minimally invasive cancer treatment. Efficient penetration of light into tissues to perform *in vivo* treatments requires the use NIR light. With their LSPRs in the NIR window, Au nanoshells, nanorods and nanocages are actively investigated (*125*).

We are exploiting plasmonic NPs to detect biomolecules and cellular signals (*126*, *127*). The LSPR peak wavelength, intensity and bandwidth can be modulated by events such as adsorption or conformational changes of molecules on NPs (*128*). NPs can provide a high spatial resolution for *in vivo* applications. Recently, transfer of chirality between chiral analyte and achiral dye molecule was demonstrated in the vicinity of a single AgNP (*129*). This can be utilized to study biomolecular processes with ultra-high resolution. Attaining single-molecule detection has been the crown jewel of SPR sensing (*130*). This is achieved by engineering highly sensitive single or an array of nanoparticles with hot spots, designing high-sensitive spectrometers, and improving a figure-of-merit (FOM, ratio of wavelength sensitivity to the line-width of LSPR). For instance, Altug and co-workers have achieved naked-eye detection of single protein monolayers by designing asymmetric Fano resonance in plasmonic nanohole arrays with a large FOM of 162 (*131*). Alternatively, Zhang and co-workers designed a zero-mode waveguide within Al nanoholes with light fields confined at the bottom to detect single-molecules (*132*). Further, rational design can be exploited to modify the emission of molecules via Purcell effect to achieve single-molecule measurements and sensing (*133*, *134*).

Metal nanoparticle arrays with plasmonic-photonic coupling have attracted interests for sensor applications due to high FOM (*135*). We have recently designed Au bowtie nanoantenna arrays (BNAs) with metal-insulator-metal (MIM) configuration to achieve high field enhancement and wide spectral response specific to sensing applications (*136*). Figure 12(a) shows the schematic of the design of the Au BNAs in MIM configuration. In this design, we can tune the spacer thickness, lattice parameters along *x-y* direction, and the bowtie gap distance for performance optimization. In particular, we have developed coordinated multiple couplings to achieve sensors with an ultra-high FOM of 254, wide refractive-index (RI) working range, and high signal-to-noise ratio. Figures 12 (b) demonstrates the sensitivity of Au BNAs with RI changing from 1 to 1.4.

The high sensitivity and compactness have motivated researchers to extend plasmonic technologies for point-of-care diagnostics. A viable strategy to achieve this is to integrate plasmonics with microfluidics (*137*, *138*). In general, label-free sensing is achieved by immobilizing a recognition element on detection substrate. For instance, a SPR sensor was used to differentiate interleukin-8 (expressing agent for prostate cancer) concentration in saliva between healthy

and cancerous individuals (*139*). In a recent study, Tamayo and co-workers have detected cancer biomarkers (carcinoembryonic antigen and the prostate specific antigen) in serum using a hybrid mechanical and optoplasmonic sensor (*139*). A detection limit of 10^{-16} gml^{-1} with very low false positives/negatives (10^{-4}) was achieved. A portable microfluidic SPR device has been developed for fast (~30 mins) detection of antibiotics (phenolic antibiotic families) in milk without any processing requirements (*140*). A similar approach has been employed to detect biotoxin (*141*). Researchers have also employed commercial SPR equipment in Kretschmann configuration to detect B-type natriuretic peptide up to 10 pg/ml (A typical range in blood is from ~20 pg/ml to 2 ng/ml) in a microfluidic channel (*142*).

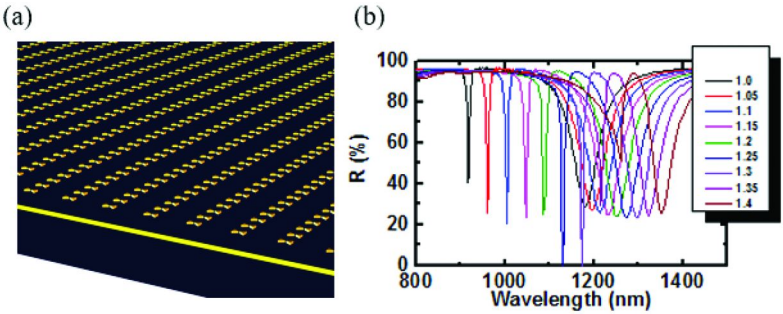

Figure 12. (a) Side view of Au BNAs with MIM configuration. (b) Normalized reflection dips of the BNAs as a function of the superstrate refractive index depicting large spectral range.

LSPR has been traditionally used in conjunction with DNA as a plasmonic ruler (*143*), and in label-free DNA biosensing (*144*). It has been extended to clinical application in biomarker detection for Alzheimer's disease (*145*) and cancer diagnostics (*146*). We have realized sensitive detection of a herbicide (paraquat) by engineering the supramolecule-modified Au NPs (*147*). We have also demonstrated the integration of an LSPR chip with a microfluidic channel to realize bulk RI sensing (*148*). Other researchers have applied LSPR-microfluidic spectroscopy to study DNA hybridization (*149*). A unique advantage of LSPR integrated with microfluidics is in the multiplexed analysis of various biomarkers. Endo et al. used specific antibodies immobilized at pre-determined locations on a nanochip containing 100 nm silica nanoparticles sandwiched between two Au films (*150*). The nanochip was utilized to detect six antigens, C-reaction protein and fibrinogen. Acimovic et al. have achieved 32 parallel sensing sites for cancer markers in serum by utilizing microfluidic systems with multiple channels (*8*) and microvalves (*151*). A similar approach was employed in real-life testing to monitor inflammatory response of infants by tracking time-course variation of their serum cytokines (*152*). The advancements in fast multiplexed sensing, along with high sensitivity, are crucial differentiators, positioning plasmonics in a unique position to create a significant impact in the biosensing industry.

5. Conclusions and Perspectives

Molecular plasmonics, which explores and exploits the interactions of plasmons with molecules, is an emerging field. It presents us with immense opportunities for basic research in multiple fields such as quantum optics, surface chemistry and molecular photonics, and for various engineering applications. Tremendous progress has been made in molecular plasmonics because of the developments in tools for molecular-scale measurements and control, nanofabrication techniques, as well as quantum and classic optical simulations. With meticulous engineering and fabrication of plasmonic nanostructures, single-molecule detection can be achieved in both SERS and LSPR sensors. Plasmonics has been exploited to improve the efficiency and reduce cost in solar-energy harvesting devices such as PEC cells and solar cells. In the healthcare sector, plasmonics has a plethora of applications such as photothermal therapy, molecular diagnosis, and *in vivo* imaging.

There has been a gradual shift from standalone devices to highly integrated lab-on-chip systems comprising of plasmonic and microfluidic components. Such plasmofluidic systems support multifunctional capabilities such as sensing, drug delivery, and molecular manipulation. A major challenge in plasmonics is the translation from a laboratory concept to real-life application. Some companies have combated this challenge and managed to create marketable products. Companies such as Renishaw Diagnostics, Carbot Corporation, and Causeway sensors are already selling SERS materials and detection methods. Major companies such as General Electric have also invested in plasmonics to create high-quality SPR sensors. Intel and IBM are forging plasmonics into information technology where plasmon-enhanced detectors and nanolasers are pursued for integrated photonic circuits. With these initial leaps, the future of plasmonics and molecular plasmonics is bright and prosperous.

References

1. Forbes. *Why IBM and Intel Are Chasing the $100B Opportunity in Nanophotonics*; 2012; available from http://www.forbes.com/sites/ joshwolfe/2012/12/13/why-ibm-and-intel-are-chasing-the-100b-opportunity-in-nanophotonics/ (accessed Jan. 15, 2016).
2. Shi, S. Y.; Chen, C. H.; Prather, D. W. Plane-wave expansion method for calculating band structure of photonic crystal slabs with perfectly matched layers. *J. Opt. Soc. Am. A*. **2004**, *21*, 1769–1775.
3. Li, Z. Y.; Lin, L. L. Photonic band structures solved by a plane-wave-based transfer-matrix method. *Phys. Rev. E* **2003**, *67*, 046607.
4. ReportLinker. *Global Markets and Technologies for Photonic Crystals*; 2015; http://www.reportlinker.com/p01105923/Global-Markets-and-Technologies-for-Photonic-Crystals.html (accessed Jan. 15, 2016).
5. Sonntag, M. D.; Klingsporn, J. M.; Zrimsek, A. B.; Sharma, B.; Ruvuna, L. K.; Van Duyne, R. P. Molecular plasmonics for nanoscale spectroscopy. *Chem. Soc. Rev.* **2014**, *43*, 1230–1247.

6. Brolo, A. G. Plasmonics for future biosensors. *Nat. Photonics* **2012**, *6*, 70–713.
7. Willets, K. A.; Van Duyne, R. P. Localized surface plasmon resonance spectroscopy and sensing. *Annu. Rev. Phys. Chem.* **2007**, *58*, 267–297.
8. Wu, Z.; Zheng, Y. Radiative Enhancement of Plasmonic Nanopatch Antennas. *Plasmonics* **2015**, 1–10.
9. Barnes, W. L.; Dereux, A.; Ebbesen, T. W. Surface plasmon subwavelength optics. *Nature* **2003**, *424*, 824–830.
10. Brockman, J. M.; Nelson, B. P.; Corn, R. M. Surface plasmon resonance imaging measurements of ultrathin organic films. *Annu. Rev. Phys. Chem.* **2000**, *51*, 41–63.
11. Stewart, M. E.; Anderton, C. R.; Thompson, L. B.; Maria, J.; Gray, S. K.; Rogers, J. A.; Nuzzo, R. G. Nanostructured plasmonic sensors. *Chem. Rev.* **2008**, *108*, 494–521.
12. Im, H.; Shao, H. L.; Park, Y. I.; Peterson, V. M.; Castro, C. M.; Weissleder, R.; Lee, H. Label-free detection and molecular profiling of exosomes with a nano-plasmonic sensor. *Nat. Biotechnol.* **2014**, *32*, 490–495.
13. Shevchenko, Y.; Camci-Unal, G.; Cuttica, D. E.; Dokmeci, M. R.; Albert, J.; Khademhosseini, A. Surface plasmon resonance fiber sensor for real-time and label-free monitoring of cellular behavior. *Biosens. Bioelectron.* **2014**, *56*, 359–367.
14. Min, C. J.; Shen, Z.; Shen, J. F.; Zhang, Y. Q.; Fang, H.; Yuan, G. H.; Du, L. P.; Zhu, S. W.; Lei, T.; Yuan, X. C. Focused plasmonic trapping of metallic particles. *Nat. Commun.* **2013**, *4*, 2891.
15. Grigorenko, A. N.; Roberts, N. W.; Dickinson, M. R.; Zhang, Y. Nanometric optical tweezers based on nanostructured substrates. *Nat. Photonics* **2008**, *2*, 365–370.
16. Li, Y.; Jing, C.; Zhang, L.; Long, Y. T. Resonance scattering particles as biological nanosensors in vitro and in vivo. *Chem. Soc. Rev.* **2012**, *41*, 632–642.
17. Noginov, M. A.; Zhu, G.; Belgrave, A. M.; Bakker, R.; Shalaev, V. M.; Narimanov, E. E.; Stout, S.; Herz, E.; Suteewong, T.; Wiesner, U. Demonstration of a spaser-based nanolaser. *Nature* **2009**, *460*, 1110–1112.
18. Tan, S. F.; Wu, L.; Yang, J. K. W.; Bai, P.; Bosman, M.; Nijhuis, C. A. Quantum Plasmon Resonances Controlled by Molecular Tunnel Junctions. *Science* **2014**, *343*, 1496–1499.
19. Russell, K. J.; Liu, T. L.; Cui, S. Y.; Hu, E. L. Large spontaneous emission enhancement in plasmonic nanocavities. *Nat. Photonics* **2012**, *6*, 459–462.
20. Whitesides, G. M.; Mathias, J. P.; Seto, C. T. Molecular Self-Assembly and Nanochemistry - a Chemical Strategy for the Synthesis of Nanostructures. *Science* **1991**, *254*, 1312–1319.
21. Love, J. C.; Estroff, L. A.; Kriebel, J. K.; Nuzzo, R. G.; Whitesides, G. M. Self-assembled monolayers of thiolates on metals as a form of nanotechnology. *Chem. Rev.* **2005**, *105*, 1103–1169.
22. Yang, S. M.; Jang, S. G.; Choi, D. G.; Kim, S.; Yu, H. K. Nanomachining by colloidal lithography. *Small* **2006**, *2*, 458–475.

23. Spinke, J.; Liley, M.; Schmitt, F. J.; Guder, H. J.; Angermaier, L.; Knoll, W. Molecular recognition at self-assembled monolayers: Optimization of surface functionalization. *J. Chem. Phys.* **1993**, *99*, 7012–7019.
24. Fan, F. R. F.; Yang, J. P.; Cai, L. T.; Price, D. W.; Dirk, S. M.; Kosynkin, D. V.; Yao, Y. X.; Rawlett, A. M.; Tour, J. M.; Bard, A. J. Charge transport through self-assembled monolayers of compounds of interest in molecular electronics. *J. Am. Chem. Soc.* **2002**, *124*, 5550–5560.
25. Chaki, N. K.; Vijayamohanan, K. Self-assembled monolayers as a tunable platform for biosensor applications. *Biosens. Bioelectron.* **2002**, *17*, 1–12.
26. Maksymovych, P.; Voznyy, O.; Dougherty, D. B.; Sorescu, D. C.; Yates, J. T. Gold adatom as a key structural component in self-assembled monolayers of organosulfur molecules on Au(111). *Prog. Surf. Sci.* **2010**, *85*, 206–240.
27. Costelle, L.; Jarvi, T. T.; Raisanen, M. T.; Tuboltsev, V.; Raisanen, J. Binding of deposited gold clusters to thiol self-assembled monolayers on Au(111) surfaces. *Appl. Phys. Lett.* **2011**, *98*, 043107.
28. Newton, L.; Slater, T.; Clark, N.; Vijayaraghavan, A. Self assembled monolayers (SAMs) on metallic surfaces (gold and graphene) for electronic applications. *J. Mater. Chem. C* **2013**, *1*, 376–393.
29. Weiss, P. S. Functional Molecules and Assemblies in Controlled Environments: Formation and Measurements. *Acc. Chem. Res.* **2008**, *41*, 1772–1781.
30. Kumar, A. S.; Ye, T.; Takami, T.; Yu, B. C.; Flatt, A. K.; Tour, J. M.; Weiss, P. S. Reversible photo-switching of single azobenzene molecules in controlled nanoscale environments. *Nano Lett.* **2008**, *8*, 1644–1648.
31. Kim, M.; Hohman, J. N.; Cao, Y.; Houk, K. N.; Ma, H.; Jen, A. K. Y.; Weiss, P. S. Creating Favorable Geometries for Directing Organic Photoreactions in Alkanethiolate Monolayers. *Science* **2011**, *331*, 1312–1315.
32. Donhauser, Z. J.; Mantooth, B. A.; Kelly, K. F.; Bumm, L. A.; Monnell, J. D.; Stapleton, J. J.; Price, D. W.; Rawlett, A. M.; Allara, D. L.; Tour, J. M.; Weiss, P. S. Conductance switching in single molecules through conformational changes. *Science* **2001**, *292*, 2303–2307.
33. Mullen, T. J.; Srinivasan, C.; Hohman, J. N.; Gillmor, S. D.; Shuster, M. J.; Horn, M. W.; Andrews, A. M.; Weiss, P. S. Microcontact insertion printing. *Appl. Phys. Lett.* **2007**, *90*, 063114.
34. Smith, R. K.; Lewis, P. A.; Weiss, P. S. Patterning self-assembled monolayers. *Prog. Surf. Sci.* **2004**, *75*, 1–68.
35. Zheng, Y. B.; Yang, Y. W.; Jensen, L.; Fang, L.; Juluri, B. K.; Flood, A. H.; Weiss, P. S.; Stoddart, J. F.; Huang, T. J. Active Molecular Plasmonics: Controlling Plasmon Resonances with Molecular Switches. *Nano Lett.* **2009**, *9*, 819–825.
36. Juluri, B. K.; Kumar, A. S.; Liu, Y.; Ye, T.; Yang, Y. W.; Flood, A. H.; Fang, L.; Stoddart, J. F.; Weiss, P. S.; Huang, T. J. A Mechanical Actuator Driven Electrochemically by Artificial Molecular Muscles. *ACS Nano* **2009**, *3*, 291–300.
37. Browne, W. R.; Feringa, B. L. Light Switching of Molecules on Surfaces. *Annu. Rev. Phys. Chem.* **2009**, *60*, 407–428.

38. Klajn, R.; Fang, L.; Coskun, A.; Olson, M. A.; Wesson, P. J.; Stoddart, J. F.; Grzybowski, B. A. Metal Nanoparticles Functionalized with Molecular and Supramolecular Switches. *J. Am. Chem. Soc.* **2009**, *131*, 4233–4235.
39. Vance, A. L.; Willey, T. M.; van Buuren, T.; Nelson, A. J.; Bostedt, C.; Fox, G. A.; Terminello, L. J. XAS and XPS characterization of a surface-attached rotaxane. *Nano Lett.* **2003**, *3*, 81–84.
40. Li, Z.; Schouteden, K.; Iancu, V.; Janssens, E.; Lievens, P.; Van Haesendonck, C.; Cerda, J. I. Chemically modified STM tips for atomic-resolution imaging of ultrathin NaCl films. *Nano Res.* **2015**, *8*, 2223–2230.
41. Ye, T.; Kumar, A. S.; Saha, S.; Takami, T.; Huang, T. J.; Stoddart, J. F.; Weiss, P. S. Changing Stations in Single Bistable Rotaxane Molecules under Electrochemical Control. *ACS Nano* **2010**, *4*, 3697–3701.
42. Kushmerick, J. G.; Holt, D. B.; Yang, J. C.; Naciri, J.; Moore, M. H.; Shashidhar, R. Metal-molecule contacts and charge transport across monomolecular layers: Measurement and theory. *Phys. Rev. Lett.* **2002**, *89*, 086802.
43. Lewis, P. A.; Inman, C. E.; Maya, F.; Tour, J. M.; Hutchison, J. E.; Weiss, P. S. Molecular engineering of the polarity and interactions of molecular electronic switches. *J. Am. Chem. Soc.* **2005**, *127*, 17421–17426.
44. Cygan, M. T.; Dunbar, T. D.; Arnold, J. J.; Bumm, L. A.; Shedlock, N. F.; Burgin, T. P.; Jones, L.; Allara, D. L.; Tour, J. M.; Weiss, P. S. Insertion, conductivity, and structures of conjugated organic oligomers in self-assembled alkanethiol monolayers on Au{111}. *J. Am. Chem. Soc.* **1998**, *120*, 2721–2732.
45. Zheng, Y. B.; Payton, J. L.; Chung, C. H.; Liu, R.; Cheunkar, S.; Pathem, B. K.; Yang, Y.; Jensen, L.; Weiss, P. S. Surface-Enhanced Raman Spectroscopy to Probe Reversibly Photoswitchable Azobenzene in Controlled Nanoscale Environments. *Nano Lett.* **2011**, *11*, 3447–3452.
46. Bumm, L. A.; Arnold, J. J.; Dunbar, T. D.; Allara, D. L.; Weiss, P. S. Electron transfer through organic molecules. *J. Phys. Chem. B* **1999**, *103*, 8122–8127.
47. Moore, A. M.; Mantooth, B. A.; Donhauser, Z. J.; Maya, F.; Price, D. W.; Yao, Y. X.; Tour, J. M.; Weiss, P. S. Cross-step place-exchange of oligo(phenylene-ethynylene) molecules. *Nano Lett.* **2005**, *5*, 2292–2297.
48. Pechenezhskiy, I. V.; Cho, J.; Nguyen, G. D.; Berbil-Bautista, L.; Giles, B. L.; Poulsen, D. A.; Frechet, J. M. J.; Crommie, M. F. Self-Assembly and Photomechanical Switching of an Azobenzene Derivative on GaAs(110): Scanning Tunneling Microscopy Study. *J. Phys. Chem. C* **2012**, *116*, 1052–1055.
49. Carroll, G. T.; London, G.; Landaluce, T. F.; Rudolf, P.; Feringa, B. L. Adhesion of Photon-Driven Molecular Motors to Surfaces via 1,3-Dipolar Cycloadditions: Effect of Interfacial Interactions on Molecular Motion. *ACS Nano* **2011**, *5*, 622–630.
50. Dri, C.; Peters, M. V.; Schwarz, J.; Hecht, S.; Grill, L. Spatial periodicity in molecular switching. *Nat. Nanotechnol.* **2008**, *3*, 649–653.

51. Zheng, Y. B.; Pathem, B. K.; Hohman, J. N.; Thomas, J. C.; Kim, M.; Weiss, P. S. Photoresponsive Molecules in Well-Defined Nanoscale Environments. *Adv. Mater.* **2013**, *25*, 302–312.
52. Wan, P. B.; Jiang, Y. G.; Wang, Y. P.; Wang, Z. Q.; Zhang, X. Tuning surface wettability through photocontrolled reversible molecular shuttle. *Chem. Commun.* **2008**, *44*, 5710–5712.
53. Baisch, B.; Raffa, D.; Jung, U.; Magnussen, O. M.; Nicolas, C.; Lacour, J.; Kubitschke, J.; Herges, R. Mounting Freestanding Molecular Functions onto Surfaces: The Platform Approach. *J. Am. Chem. Soc.* **2009**, *131*, 442–443.
54. Jacob, H.; Ulrich, S.; Jung, U.; Lemke, S.; Rusch, T.; Schutt, C.; Petersen, F.; Strunskus, T.; Magnussen, O.; Herges, R.; Tuczek, F. Monitoring the reversible photoisomerization of an azobenzene-functionalized molecular triazatriangulene platform on Au(111) by IRRAS. *Phys. Chem. Chem. Phys.* **2014**, *16*, 22643–22650.
55. Kneipp, K.; Wang, Y.; Kneipp, H.; Perelman, L. T.; Itzkan, I.; Dasari, R.; Feld, M. S. Single molecule detection using surface-enhanced Raman scattering (SERS). *Phys. Rev. Lett.* **1997**, *78*, 1667–1670.
56. Schlucker, S. Surface-Enhanced Raman Spectroscopy: Concepts and Chemical Applications. *Angew. Chem. Int. Ed.* **2014**, *53*, 4756–4795.
57. Tripp, R. A.; Dluhy, R. A.; Zhao, Y. P. Novel nanostructures for SERS biosensing. *Nano Today* **2008**, *3*, 31–37.
58. Stevenson, R.; Ingram, A.; Leung, H.; McMillan, D. C.; Graham, D. Quantitative SERRS immunoassay for the detection of human PSA. *Analyst* **2009**, *134*, 842–844.
59. Song, J. B.; Zhou, J. J.; Duan, H. W. Self-Assembled Plasmonic Vesicles of SERS-Encoded Amphiphilic Gold Nanoparticles for Cancer Cell Targeting and Traceable Intracellular Drug Delivery. *J. Am. Chem. Soc.* **2012**, *134*, 13458–13469.
60. Zengin, A.; Tamer, U.; Caykara, T. A SERS-Based Sandwich Assay for Ultrasensitive and Selective Detection of Alzheimer's Tau Protein. *Biomacromolecules* **2013**, *14*, 3001–3009.
61. Choi, I.; Huh, Y. S.; Erickson, D. Ultra-sensitive, label-free probing of the conformational characteristics of amyloid beta aggregates with a SERS active nanofluidic device. *Microfluid. Nanofluid.* **2012**, *12*, 663–669.
62. Paxton, W. F.; Kleinman, S. L.; Basuray, A. N.; Stoddart, J. F.; Van Duyne, R. P. Surface-enhanced Raman spectroelectrochemistry of TTF-modified self-assembled monolayers. *J. Phys. Chem. Lett.* **2011**, *2*, 1145–1149.
63. Stuart, D. A.; Biggs, K. B.; Van Duyne, R. P. Surface-enhanced Raman spectroscopy of half-mustard agent. *Analyst* **2006**, *131*, 568–572.
64. Radziuk, D.; Moehwald, H. Prospects for plasmonic hot spots in single molecule SERS towards the chemical imaging of live cells. *Phys. Chem. Chem. Phys.* **2015**, *17*, 21072–21093.
65. Tuma, R. Raman spectroscopy of proteins: from peptides to large assemblies. *J. Raman Spectrosc.* **2005**, *36*, 307–319.
66. Moskovits, M.; Suh, J. S. Surface Selection-Rules for Surface-Enhanced Raman-Spectroscopy - Calculations and Application to the Surface-

Enhanced Raman-Spectrum of Phthalazine on Silver. *J. Phys. Chem.* **1984**, *88*, 5526–5530.
67. Moskovits, M.; Dilella, D. P.; Maynard, K. J. Surface Raman-Spectroscopy of a Number of Cyclic Aromatic-Molecules Adsorbed on Silver - Selection-Rules and Molecular-Reorientation. *Langmuir* **1988**, *4*, 67–76.
68. Comstock, M. J.; Levy, N.; Kirakosian, A.; Cho, J.; Lauterwasser, F.; Harvey, J. H.; Strubbe, D. A.; Frechet, J. M. J.; Trauner, D.; Louie, S. G.; Crommie, M. F. Reversible photomechanical switching of individual engineered molecules at a metallic surface. *Phys. Rev. Lett.* **2007**, *99*, 178301.
69. Witlicki, E. H.; Johnsen, C.; Hansen, S. W.; Silverstein, D. W.; Bottomley, V. J.; Jeppesen, J. O.; Wong, E. W.; Jensen, L.; Flood, A. H. Molecular Logic Gates Using Surface-Enhanced Raman-Scattered Light. *J. Am. Chem. Soc.* **2011**, *133*, 7288–7291.
70. Zheng, Y. B.; Payton, J. L.; Song, T. B.; Pathem, B. K.; Zhao, Y. X.; Ma, H.; Yang, Y.; Jensen, L.; Jen, A. K. Y.; Weiss, P. S. Surface-Enhanced Raman Spectroscopy To Probe Photoreaction Pathways and Kinetics of Isolated Reactants on Surfaces: Flat versus Curved Substrates. *Nano Lett.* **2012**, *12*, 5362–5368.
71. Keller, E. L.; Brandt, N. C.; Cassabaum, A. A.; Frontiera, R. R. Ultrafast surface-enhanced Raman spectroscopy. *Analyst* **2015**, *140*, 4922–4931.
72. Shiohara, A.; Wang, Y.; Liz-Marzán, L. M. Recent approaches toward creation of hot spots for SERS detection. *J. Photochem. Photobiol., C* **2014**, *21*, 2–25.
73. Zhang, G.; Wang, D. Colloidal lithography—the art of nanochemical patterning. *Chem. Asian. J.* **2009**, *4*, 236–245.
74. Hulteen, J. C.; Van Duyne, R. P. Nanosphere lithography: a materials general fabrication process for periodic particle array surfaces. *J. Vac. Sci. Technol., A* **1995**, *13*, 1553–1558.
75. Haynes, C. L.; Van Duyne, R. P. Nanosphere lithography: A versatile nanofabrication tool for studies of size-dependent nanoparticle optics. *J. Phys. Chem. B* **2001**, *105*, 5599–5611.
76. Choi, J.-Y.; Alford, T.; Honsberg, C. B. Solvent-controlled spin-coating method for large-scale area deposition of two-dimensional silica nanosphere assembled layers. *Langmuir* **2014**, *30*, 5732–5738.
77. Zheng, Y. B.; Jensen, L.; Yan, W.; Walker, T. R.; Juluri, B. K.; Jensen, L.; Huang, T. J. Chemically tuning the localized surface plasmon resonances of gold nanostructure arrays. *J. Phys. Chem. C* **2009**, *113*, 7019–7024.
78. Zheng, Y. B.; Juluri, B. K.; Mao, X.; Walker, T. R.; Huang, T. J. Systematic investigation of localized surface plasmon resonance of long-range ordered Au nanodisk arrays. *J. Appl. Phys.* **2008**, *103*, 014308.
79. Kosiorek, A.; Kandulski, W.; Glaczynska, H.; Giersig, M. Fabrication of nanoscale rings, dots, and rods by combining shadow nanosphere lithography and annealed polystyrene nanosphere masks. *Small* **2005**, *1*, 439–444.
80. Huang, Z.; Fang, H.; Zhu, J. Fabrication of silicon nanowire arrays with controlled diameter, length, and density. *Adv. Mater.* **2007**, *19*, 744–748.

81. Li, Y.; Zhang, J.; Zhu, S.; Dong, H.; Wang, Z.; Sun, Z.; Guo, J.; Yang, B. Bioinspired silicon hollow-tip arrays for high performance broadband anti-reflective and water-repellent coatings. *J. Mater. Chem.* **2009**, *19*, 1806–1810.
82. Lee, S. H.; Bantz, K. C.; Lindquist, N. C.; Oh, S.-H.; Haynes, C. L. Self-assembled plasmonic nanohole arrays. *Langmuir* **2009**, *25*, 13685–13693.
83. Zheng, Y. B.; Juluri, B. K.; Kiraly, B.; Huang, T. J. Ordered Au Nanodisk and Nanohole Arrays: Fabrication and Applications. *J. Nanotechnol. Eng. Med.* **2010**, *1*, 031011.
84. Haynes, C. L.; McFarland, A. D.; Smith, M. T.; Hulteen, J. C.; Van Duyne, R. P. Angle-resolved nanosphere lithography: Manipulation of nanoparticle size, shape, and interparticle spacing. *J. Phys. Chem. B* **2002**, *106*, 1898–1902.
85. Kosiorek, A.; Kandulski, W.; Chudzinski, P.; Kempa, K.; Giersig, M. Shadow nanosphere lithography: simulation and experiment. *Nano Lett.* **2004**, *4*, 1359–1363.
86. Honda, M.; Kumamoto, Y.; Taguchi, A.; Saito, Y.; Kawata, S. Plasmon-enhanced UV photocatalysis. *Appl. Phys. Lett.* **2014**, *104*, 061108.
87. Haes, A. J.; Van Duyne, R. P. A nanoscale optical biosensor: sensitivity and selectivity of an approach based on the localized surface plasmon resonance spectroscopy of triangular silver nanoparticles. *J. Am. Chem. Soc.* **2002**, *124*, 10596–10604.
88. Zheng, Y. B.; Juluri, B. K.; Jensen, L. L.; Ahmed, D.; Lu, M. Q.; Jensen, L.; Huang, T. J. Dynamic Tuning of Plasmon-Exciton Coupling in Arrays of Nanodisk-J-aggregate Complexes. *Adv. Mater.* **2010**, *22*, 3603–3607.
89. Liu, Y. J.; Zheng, Y. B.; Liou, J.; Chiang, I. K.; Khoo, I. C.; Huang, T. J. All-Optical Modulation of Localized Surface Plasmon Coupling in a Hybrid System Composed of Photoswitchable Gratings and Au Nanodisk Arrays. *J. Phys. Chem. C* **2011**, *115*, 7717–7722.
90. Chen, K.; Rajeeva, B. B.; Wu, Z.; Rukavina, M.; Dao, T. D.; Ishii, S.; Aono, M.; Nagao, T.; Zheng, Y. Moiré Nanosphere Lithography. *ACS Nano* **2015**, *9*, 6031–6040.
91. Wu, Z.; Chen, K.; Menz, R.; Nagao, T.; Zheng, Y. Tunable multiband metasurfaces by moiré nanosphere lithography. *Nanoscale* **2015**, *7*, 20391–20396.
92. Paz, V. F.; Emons, M.; Obata, K.; Ovsianikov, A.; Peterhansel, S.; Frenner, K.; Reinhardt, C.; Chichkov, B.; Morgner, U.; Osten, W. Development of functional sub-100 nm structures with 3D two-photon polymerization technique and optical methods for characterization. *J. Laser Appl.* **2012**, *24*, 042004.
93. Ergin, T.; Stenger, N.; Brenner, P.; Pendry, J. B.; Wegener, M. Three-Dimensional Invisibility Cloak at Optical Wavelengths. *Science* **2010**, *328*, 337–339.
94. Chen, H. J.; Ming, T. A.; Zhao, L.; Wang, F.; Sun, L. D.; Wang, J. F.; Yan, C. H. Plasmon-molecule interactions. *Nano Today* **2010**, *5*, 494–505.

95. Ueno, K.; Takabatake, S.; Nishijima, Y.; Mizeikis, V.; Yokota, Y.; Misawa, H. Nanogap-Assisted Surface Plasmon Nanolithography. *J. Phys. Chem. Lett.* **2010**, *1*, 657–662.
96. Gruber, C.; Hirzer, A.; Schmidt, V.; Trugler, A.; Hohenester, U.; Ditlbacher, H.; Hohenau, A.; Krenn, J. R. Imaging nanowire plasmon modes with two-photon polymerization. *Appl. Phys. Lett.* **2015**, *106*, 081101.
97. Diebold, E. D.; Peng, P.; Mazur, E. Isolating Surface-Enhanced Raman Scattering Hot Spots Using Multiphoton Lithography. *J. Am. Chem. Soc.* **2009**, *131*, 16356–16357.
98. Deeb, C.; Zhou, X.; Gérard, D.; Bouhelier, A.; Jain, P. K.; Plain, J.; Soppera, O.; Royer, P.; Bachelot, R. Off-resonant optical excitation of gold nanorods: nanoscale imprint of polarization surface charge distribution. *J. Phys. Chem. Lett.* **2010**, *2*, 7–11.
99. Rajeeva, B. B.; Hernandez, D. S.; Wang, M.; Perillo, E.; Lin, L.; Scarabelli, L.; Pingali, B.; Liz-Marzán, L. M.; Dunn, A. K.; Shear, J. B. Regioselective Localization and Tracking of Biomolecules on Single Gold Nanoparticles. *Adv. Sci.* **2015**, *2*.
100. Pitts, J. D.; Campagnola, P. J.; Epling, G. A.; Goodman, S. L. Submicron multiphoton free-form fabrication of proteins and polymers: Studies of reaction efficiencies and applications in sustained release. *Macromolecules* **2000**, *33*, 1514–1523.
101. Sun, Y.-L.; Dong, W.-F.; Niu, L.-G.; Jiang, T.; Liu, D.-X.; Zhang, L.; Wang, Y.-S.; Chen, Q.-D.; Kim, D.-P.; Sun, H.-B. Protein-based soft micro-optics fabricated by femtosecond laser direct writing. *Light Sci. Appl.* **2014**, *3*, e129.
102. PersistenceMarketResearch. *Global Market Study on Biosensor: Asia-Pacific to Witness Highest Growth by 2020*; 2015; http://www.persistencemarketresearch.com/market-research/biosensor-market.asp (accessed Jan. 15, 2016).
103. Fujishima, A.; Honda, K. Photolysis-decomposition of water at the surface of an irradiated semiconductor. *Nature* **1972**, *238*, 37–38.
104. Linic, S.; Christopher, P.; Ingram, D. B. Plasmonic-metal nanostructures for efficient conversion of solar to chemical energy. *Nat. Mater.* **2011**, *10*, 911–921.
105. Pu, Y. C.; Wang, G. M.; Chang, K. D.; Ling, Y. C.; Lin, Y. K.; Fitzmorris, B. C.; Liu, C. M.; Lu, X. H.; Tong, Y. X.; Zhang, J. Z.; Hsu, Y. J.; Li, Y. Au Nanostructure-Decorated TiO_2 Nanowires Exhibiting Photoactivity Across Entire UV-visible Region for Photoelectrochemical Water Splitting. *Nano Lett.* **2013**, *13*, 3817–3823.
106. Chen, H. M.; Chen, C. K.; Tseng, M. L.; Wu, P. C.; Chang, C. M.; Cheng, L. C.; Huang, H. W.; Chan, T. S.; Huang, D. W.; Liu, R. S.; Tsai, D. P. Plasmonic ZnO/Ag Embedded Structures as Collecting Layers for Photogenerating Electrons in Solar Hydrogen Generation Photoelectrodes. *Small* **2013**, *9*, 2926–2936.
107. Zhou, L.; Yu, X. Q.; Zhu, J. Metal-Core/Semiconductor-Shell Nanocones for Broadband Solar Absorption Enhancement. *Nano Lett.* **2014**, *14*, 1093–1098.

108. Warren, S. C.; Thimsen, E. Plasmonic solar water splitting. *Energ. Environ. Sci.* **2012**, *5*, 5133–5146.
109. Liu, Z. W.; Hou, W. B.; Pavaskar, P.; Aykol, M.; Cronin, S. B. Plasmon Resonant Enhancement of Photocatalytic Water Splitting Under Visible Illumination. *Nano Lett.* **2011**, *11*, 1111–1116.
110. Zhang, X.; Liu, Y.; Lee, S. T.; Yang, S. H.; Kang, Z. H. Coupling surface plasmon resonance of gold nanoparticles with slow-photon-effect of TiO_2 photonic crystals for synergistically enhanced photoelectrochemical water splitting. *Energy Environ. Sci.* **2014**, *7*, 1409–1419.
111. Chen, H. M.; Chen, C. K.; Chen, C. J.; Cheng, L. C.; Wu, P. C.; Cheng, B. H.; Ho, Y. Z.; Tseng, M. L.; Hsu, Y. Y.; Chan, T. S.; Lee, J. F.; Liu, R. S.; Tsai, D. P. Plasmon Inducing Effects for Enhanced Photoelectrochemical Water Splitting: X-ray Absorption Approach to Electronic Structures. *ACS Nano* **2012**, *6*, 7362–7372.
112. Primo, A.; Marino, T.; Corma, A.; Molinari, R.; Garcia, H. Efficient Visible-Light Photocatalytic Water Splitting by Minute Amounts of Gold Supported on Nanoparticulate CeO_2 Obtained by a Biopolymer Templating Method. *J. Am. Chem. Soc.* **2011**, *133*, 6930–6933.
113. Chen, X. Q.; Li, P.; Tong, H.; Kako, T.; Ye, J. H. Nanoarchitectonics of a Au nanoprism array on WO_3 film for synergistic optoelectronic response. *Sci. Technol. Adv. Mater.* **2011**, *12*, 044604.
114. Chen, H. M.; Chen, C. K.; Liu, R. S.; Zhang, L.; Zhang, J. J.; Wilkinson, D. P. Nano-architecture and material designs for water splitting photoelectrodes. *Chem. Soc. Rev.* **2012**, *41*, 5654–5671.
115. Zhang, P.; Wang, T.; Gong, J. Mechanistic Understanding of the Plasmonic Enhancement for Solar Water Splitting. *Adv. Mat.* **2015**, *27*, 5328–5342.
116. Park, Y.; McDonald, K. J.; Choi, K. S. Progress in bismuth vanadate photoanodes for use in solar water oxidation. *Chem. Soc. Rev.* **2013**, *42*, 2321–2337.
117. Kim, T. W.; Choi, K. S. Nanoporous $BiVO_4$ Photoanodes with Dual-Layer Oxygen Evolution Catalysts for Solar Water Splitting. *Science* **2014**, *343*, 990–994.
118. Gan, J.; Lu, X.; Rajeeva, B. B.; Menz, R.; Tong, Y.; Zheng, Y. Efficient Photoelectrochemical Water Oxidation over Hydrogen-Reduced Nanoporous $BiVO_4$ with Ni–Bi Electrocatalyst. *ChemElectroChem* **2015**, *2*, 1385–1395.
119. Zhang, L. W.; Lin, C. Y.; Valev, V. K.; Reisner, E.; Steiner, U.; Baumberg, J. J. Plasmonic Enhancement in $BiVO_4$ Photonic Crystals for Efficient Water Splitting. *Small* **2014**, *10*, 3970–3978.
120. Gan, J.; Rajeeva, B. B.; Wu, Z. L.; Tong, Y. X.; Zheng, Y. B. Plasmon-Induced Hot-Electron and Energy Transfer Enhancement in Nanoporous $BiVO_4$ for Efficient Photoelectrochemical Water Oxidation. Submitted for publication, 2015.
121. Atwater, H. A.; Polman, A. Plasmonics for improved photovoltaic devices. *Nat. Mater.* **2010**, *9*, 205–213.
122. Ellmer, K. Past achievements and future challenges in the development of optically transparent electrodes. *Nat. Photonics* **2012**, *6*, 809–817.

123. Chen, C.-C.; Dou, L.; Zhu, R.; Chung, C.-H.; Song, T.-B.; Zheng, Y. B.; Hawks, S.; Li, G.; Weiss, P. S.; Yang, Y. Visibly transparent polymer solar cells produced by solution processing. *ACS Nano* **2012**, *6*, 7185–7190.
124. Rajeeva, B. B.; Menz, R.; Zheng, Y. Towards rational design of multifunctional theranostic nanoparticles: what barriers do we need to overcome? *Nanomedicine (London)* **2014**, *9*, 1767–1770.
125. Huang, X.; Jain, P. K.; El-Sayed, I. H.; El-Sayed, M. A. Plasmonic photothermal therapy (PPTT) using gold nanoparticles. *Laser Med. Sci.* **2008**, *23*, 217–228.
126. Guo, L.; Kim, D.-H. LSPR biomolecular assay with high sensitivity induced by aptamer–antigen–antibody sandwich complex. *Biosens. Bioelectron.* **2012**, *31*, 567–570.
127. Oh, B.-R.; Huang, N.-T.; Chen, W.; Seo, J. H.; Chen, P.; Cornell, T. T.; Shanley, T. P.; Fu, J.; Kurabayashi, K. Integrated nanoplasmonic sensing for cellular functional immunoanalysis using human blood. *ACS Nano* **2014**, *8*, 2667–2676.
128. Hsiao, V. K.; Zheng, Y. B.; Juluri, B. K.; Huang, T. J. Light-driven plasmonic switches based on au nanodisk arrays and photoresponsive liquid crystals. *Adv. Mater.* **2008**, *20*, 3528–3532.
129. Pour, S. O.; Rocks, L.; Faulds, K.; Graham, D.; Parchansky, V.; Bour, P.; Blanch, E. W. Through-space transfer of chiral information mediated by a plasmonic nanomaterial. *Nat. Chem.* **2015**, *7*, 591–596.
130. Mayer, K. M.; Hao, F.; Lee, S.; Nordlander, P.; Hafner, J. H. A single molecule immunoassay by localized surface plasmon resonance. *Nanotechnology* **2010**, *21*, 255503.
131. Yanik, A. A.; Cetin, A. E.; Huang, M.; Artar, A.; Mousavi, S. H.; Khanikaev, A.; Connor, J. H.; Shvets, G.; Altug, H. Seeing protein monolayers with naked eye through plasmonic Fano resonances. *Proc. Natl. Acad. Sci. U.S.A.* **2011**, *108*, 11784–11789.
132. Zhao, C. L.; Liu, Y. M.; Yang, J.; Zhang, J. S. Single-molecule detection and radiation control in solutions at high concentrations via a heterogeneous optical slot antenna. *Nanoscale* **2014**, *6*, 9103–9109.
133. Cang, H.; Liu, Y. M.; Wang, Y.; Yin, X. B.; Zhang, X. Giant Suppression of Photobleaching for Single Molecule Detection via the Purcell Effect. *Nano Lett.* **2013**, *13*, 5949–5953.
134. Kinkhabwala, A.; Yu, Z. F.; Fan, S. H.; Avlasevich, Y.; Mullen, K.; Moerner, W. E. Large single-molecule fluorescence enhancements produced by a bowtie nanoantenna. *Nat. Photonics* **2009**, *3*, 654–657.
135. Shen, Y.; Zhou, J. H.; Liu, T. R.; Tao, Y. T.; Jiang, R. B.; Liu, M. X.; Xiao, G. H.; Zhu, J. H.; Zhou, Z. K.; Wang, X. H.; Jin, C. J.; Wang, J. F. Plasmonic gold mushroom arrays with refractive index sensing figures of merit approaching the theoretical limit. *Nat. Commun.* **2013**, *4*, 2381.
136. Lin, L.; Zheng, Y. Optimizing plasmonic nanoantennas via coordinated multiple coupling. *Sci. Rep.* **2015**, *5*, 14788.
137. Wang, M. S.; Zhao, C. L.; Miao, X. Y.; Zhao, Y. H.; Rufo, J.; Liu, Y. J.; Huang, T. J.; Zheng, Y. B. Plasmofluidics: Merging Light and Fluids at the Micro-/Nanoscale. *Small* **2015**, *11*, 4423–4444.

138. Niu, L.; Zhang, N.; Liu, H.; Zhou, X.; Knoll, W. Integrating plasmonic diagnostics and microfluidics. *Biomicrofluidics* **2015**, *9*, 052611.
139. Kosaka, P. M.; Pini, V.; Ruz, J. J.; da Silva, R. A.; Gonzalez, M. U.; Ramos, D.; Calleja, M.; Tamayo, J. Detection of cancer biomarkers in serum using a hybrid mechanical and optoplasmonic nanosensor. *Nat. Nanotechnol.* **2014**, *9*, 1047–1053.
140. Fernandez, F.; Hegnerova, K.; Piliarik, M.; Sanchez-Baeza, F.; Homola, J.; Marco, M. P. A label-free and portable multichannel surface plasmon resonance immunosensor for on site analysis of antibiotics in milk samples. *Biosens. Bioelectron.* **2010**, *26*, 1231–1238.
141. Feltis, B. N.; Sexton, B. A.; Glenn, F. L.; Best, M. J.; Wilkins, M.; Davis, T. J. A hand-held surface plasmon resonance biosensor for the detection of ricin and other biological agents. *Biosens. Bioelectron.* **2008**, *23*, 1131–1136.
142. Kurita, R.; Yokota, Y.; Sato, Y.; Mizutani, F.; Niwa, O. On-chip enzyme immunoassay of a cardiac marker using a microfluidic device combined with a portable surface plasmon resonance system. *Anal. Chem.* **2006**, *78*, 5525–5531.
143. Sonnichsen, C.; Reinhard, B. M.; Liphardt, J.; Alivisatos, A. P. A molecular ruler based on plasmon coupling of single gold and silver nanoparticles. *Nat. Biotechnol.* **2005**, *23*, 741–745.
144. Endo, T.; Kerman, K.; Nagatani, N.; Takamura, Y.; Tamiya, E. Label-free detection of peptide nucleic acid-DNA hybridization using localized surface plasmon resonance based optical biosensor. *Anal. Chem.* **2005**, *77*, 6976–6984.
145. Haes, A. J.; Chang, L.; Klein, W. L.; Van Duyne, R. P. Detection of a biomarker for Alzheimer's disease from synthetic and clinical samples using a nanoscale optical biosensor. *J. Am. Chem. Soc.* **2005**, *127*, 2264–2271.
146. El-Sayed, I. H.; Huang, X. H.; El-Sayed, M. A. Surface plasmon resonance scattering and absorption of anti-EGFR antibody conjugated gold nanoparticles in cancer diagnostics: Applications in oral cancer. *Nano Lett.* **2005**, *5*, 829–834.
147. Li, H.; Chen, D. X.; Sun, Y. L.; Zheng, Y. B.; Tan, L. L.; Weiss, P. S.; Yang, Y. W. Viologen-mediated assembly of and sensing with carboxylatopillar[5]arene-modified gold nanoparticles. *J. Am. Chem. Soc.* **2013**, *135*, 1570–1576.
148. Zheng, Y. B.; Juluri, B. K.; Mao, X. L.; Walker, T. R.; Huang, T. J. Systematic investigation of localized surface plasmon resonance of long-range ordered Au nanodisk arrays. *J. Appl. Phys.* **2008**, *103*, 014308.
149. Huang, C.; Ye, J.; Wang, S.; Stakenborg, T.; Lagae, L. Gold nanoring as a sensitive plasmonic biosensor for on-chip DNA detection. *Appl. Phys. Lett.* **2012**, *100*, 173114.
150. Endo, T.; Kerman, K.; Nagatani, N.; Hiepa, H. M.; Kim, D.-K.; Yonezawa, Y.; Nakano, K.; Tamiya, E. Multiple label-free detection of antigen-antibody reaction using localized surface plasmon resonance-based core-shell structured nanoparticle layer nanochip. *Anal. Chem.* **2006**, *78*, 6465–6475.

151. Acimovic, S. S.; Ortega, M. A.; Sanz, V.; Berthelot, J.; Garcia-Cordero, J. L.; Renger, J.; Maerkl, S. J.; Kreuzer, M. P.; Quidant, R. LSPR Chip for Parallel, Rapid, and Sensitive Detection of Cancer Markers in Serum. *Nano Lett.* **2014**, *14*, 2636–2641.
152. Chen, P. Y.; Chung, M. T.; McHugh, W.; Nidetz, R.; Li, Y. W.; Fu, J. P.; Cornell, T. T.; Shanley, T. P.; Kurabayashi, K. Multiplex Serum Cytokine Immunoassay Using Nanoplasmonic Biosensor Microarrays. *ACS Nano* **2015**, *9*, 4173–4181.